Available online at www.sciencedirect.com
SCIENCE DIRECT®
Nuclear Physics B 743 [FS] (2006) 249–275
NUCLEAR PHYSICS B

Casimir effects: An optical approach II. Local observables and thermal corrections

A. Scardicchio , R.L. Jaffe

Center for Theoretical Physics, Laboratory for Nuclear Sciences and Physics Department, Massachusetts Institute of Technology, Cambridge, MA 02139, USA

Received 5 October 2005; received in revised form 3 February 2006; accepted 22 February 2006

Available online 20 March 2006

Abstract

We recently proposed a new approach to the Casimir effect based on classical ray optics (the "optical approximation"). In this paper we show how to use it to calculate the local observables of the field theory. In particular, we study the energy–momentum tensor and the Casimir pressure. We work three examples in detail: parallel plates, the Casimir pendulum and a sphere opposite a plate. We also show how to calculate thermal corrections, proving that the high temperature 'classical limit' is indeed valid for any smooth geometry.

PACS: 03.65.Sq; 03.70.+k; 42.25.Gy

1. Introduction

The Casimir effect [1–5] is a manifestation of the quantum fluctuations of a quantum field at a macroscopic level. Experiments on Casimir forces are precise tests of one of the less intuitive predictions of field theory. For a theoretician, predicting the outcome of these experiments is a worthy challenge. Hence it seems somewhat astonishing that an exact solution exists only for infinite, parallel plates case [1]. Other formal solutions for geometries not made of distinct rigid bodies free to move (like the wedge, the interior of a sphere or of a rectangular box [3]) are irrelevant for an experimental setup. Moreover in many such solutions divergences have been discarded in a way that leaves the result unrelated to practical materials and configurations [6].

* Corresponding author.
E-mail addresses: scardicc@mit.edu (A. Scardicchio), jaffe@mit.edu (R.L. Jaffe).

0550-3213/$ – see front matter
doi:10.1016/j.nuclphysb.2006.02.038

Interesting theoretical developments include the method developed in [7] where the solution for infinite periodic geometries is obtained as a series expansion in the corrugation, and the numerical Monte Carlo analysis in [8].

Amongst the various effects that an experimentalist must take in account to interpret the data (e.g. finite conductivity, temperature and roughness corrections) probably the most challenging, interesting and full of connections with other branches of physics and mathematics is the dependence of the force on the geometry of the bodies. Calculating the Casimir force for perfectly reflecting bodies in the end reduces to finding the density of states (DOS) of the Schrödinger Hamiltonian for the equivalent billiard problem *including the oscillatory ripple on the averaged DOS*. This is an incredibly difficult problem in spectral theory that still challenges mathematicians and physicists today [9] and in essence is not solved beyond the semiclassical approximation.

In this context we have introduced in Refs. [10,11] a method based on classical optics which has several virtues: accuracy, uniform validity when a symmetry is born, straightforward extension to higher spin fields, to non-zero temperatures, to include finite reflectivity and, the main topic of this paper, *it can provide an approximation to local observables*.

This paper is structured as follows: in Section 2 we show how to cast the energy–momentum tensor into a sum over optical paths contributions and how to regulate and analyze the divergences, ubiquitous in Casimir energy calculations. Section 3 is dedicated to the analysis of the three examples already studied in [11] with pedagogical intent. We study parallel plates, the Casimir torsion pendulum and a sphere opposite a plate. In Section 4 we show how to calculate the same local observables and the free energy for a thermal state and we prove (within the limits of our approximation) the 'classical limit' theorem [4,13], which states that at high T, Casimir forces become independent of h and proportional to T. As far as we know this is the first time this assertion can be generalized to geometries other than parallel plates. We also study the example of parallel plates (finding the known results) and of a sphere opposite a plate at non-zero temperature. We find evidence, again within the framework of the optical approximation, that the low T behavior of the Casimir force is a difficult problem, qualitatively different from the $\mathsf{T} = 0$ and high temperature cases.

2. Local observables

Local properties of the quantum vacuum induced by the presence of boundaries are of broad interest in quantum field theory [14]. For example, gravity couples locally to the energy–momentum tensor. Vacuum polarization induces local charge densities near boundaries, provided the symmetries of the theory allow it. Also, local densities are free from some of the cutoff dependencies that plague many other Casimir effects. Any local observable that can 9(thatimir893(stat88 .)-2

2.1. Energy–momentum tensor

We study the Noether energy–momentum tensor of a free, real scalar field φ in a domain $\mathcal{D}$ with Dirichlet boundary conditions (BC) on $\mathcal{S} = \partial\mathcal{D}$ made of (in general disconnected) surfaces. Other BC (Neumann, Robin) can be discussed but for simplicity we restrict ourselves to Dirichlet BC here.

The Lagrangian is (we use $\hbar = c = 1$)

$$\mathcal{L} = \frac{1}{2}\partial_\mu\varphi\partial^\mu\varphi - \frac{1}{2}m^2\varphi^2, \tag{2.1}$$

where Greek letters are used for 4-dimensional indices while the vector notation will be used for spatial vectors.

The Noether energy–momentum tensor for this real scalar field is

$$T_{\mu\nu} = \frac{\partial\mathcal{L}}{\partial(\partial^\mu\varphi)}\partial_\nu\varphi - g_{\mu\nu}\mathcal{L}, \tag{2.2}$$

$$T_{\mu\nu} = \partial_\mu\varphi\,\partial_\nu\varphi - g_{\mu\nu}\frac{1}{2}\left(\partial_\alpha\varphi\,\partial^\alpha\varphi - m^2\varphi^2\right) \tag{2.3}$$

from which we identify the energy density T_{00}, the momentum density T_{0i}, and the stress tensor T_{ij}. The definition of these quadratic operators involves divergences that we will regulate by point splitting. We hence replace quadratic operators like $\varphi(x)^2$ by $\lim_{x'\to x}\varphi(x')\varphi(x)$. The energy density operator, for example, is

$$\begin{aligned} T_{00}(x,t) &= \lim_{x'\to x}\left[\frac{1}{2}\partial_0\varphi(x',t)\partial_0\varphi(x,t) + \frac{1}{2}\vec{\nabla}'\cdot\vec{\nabla}\varphi(x',t)\varphi(x,t) + \frac{1}{2}m^2\varphi(x',t)\varphi(x,t)\right] \\ &= \lim_{x'\to x}\left[\frac{1}{2}\partial_0\varphi(x',t)\partial_0\varphi(x,t) - \frac{1}{2}\varphi(x',t)\vec{\nabla}^2\varphi(x,t)\right. \\ &\quad \left. + \frac{1}{2}m^2\varphi(x',t)\varphi(x,t) + \frac{1}{2}(\vec{\nabla}' + \vec{\nabla})\cdot\varphi(x',t)\vec{\nabla}\varphi(x,t)\right]. \end{aligned} \tag{2.4}$$

The field φ satisfies the free wave equation in $\mathcal{D}$

$$\partial^2\varphi + m^2\varphi = 0 \tag{2.5}$$

and hence it can be decomposed into normal modes

$$\varphi(x,t) = \sum_j \frac{1}{\sqrt{2E_j}}\left(\psi_j(x)e^{-iE_jt}a_j + \psi_j(x)e^{iE_jt}a_j^\dagger\right), \tag{2.6}$$

where ψ_j and E_j are the eigenfunctions and eigenvalues of the problem

$$\left(-\vec{\nabla}^2 + m^2\right)\psi_j = E_j^2\psi_j \quad \text{for } x\in\mathcal{D}, \quad \psi_j(x) = 0 \quad \text{for } x\in\mathcal{S}. \tag{2.7}$$

We also use the definition $E(k) = \sqrt{k^2+m^2}$, and $E_j = \sqrt{k_j^2+m^2}$ so that the eigenvalue equation reads

$$-\vec{\nabla}^2\psi_j = k_j^2\psi_j\,, \tag{2.8}$$

and because of the positivity of the operator $-\vec{\nabla}^2$, the spectrum $\{E_j\}$ is contained in the half-line $\{E \geqslant m\}$.

We now introduce the propagator $G(x', x, k)$, defined as in Ref. [11] to be the Green's function of the problem (2.7) or (2.8):

$$\begin{aligned} &\left(-\vec{\nabla}'^2 - k^2\right) G(x', x, k) = \delta(x' - x), \\ &G(x', x) = 0 \quad \text{for } x' \quad \text{or} \quad x \in \mathcal{S}, \end{aligned} \tag{2.9}$$

which can be written using the spectral decomposition as

$$G(x', x, k) = \sum_n \frac{\psi_n(x')\psi_n(x)}{k_n^2 - k^2 - i\square}. \tag{2.10}$$

In Ref. [10] we have developed an approximation for the propagator $G(x', x, k)$ in terms of optical paths (closed, in the limit $x' \to x$). The derivation can be found in Ref. [11], the general result valid for N spatial dimensions being

$$\begin{aligned} G_{\text{opt}}(x', x, k) = &\sum_r \frac{(-1)^{n_r}}{2^{N/2+1}\pi^{N/2-1}} (\square_r \Delta_r)^{1/2} k^{N/2-1} H^{(1)}_{\frac{N}{2}-1}(k\square_r), \\ &\sum_r G_r(x', x, k), \end{aligned} \tag{2.11}$$

where H is a Hankel function, r labels the paths from x to x', n_r is the number of reflections of the path r, $\square_r(x', x)$ is its length and $\Delta_r(x', x)$ is the *enlargement factor* familiar from classical optics,

$$\Delta_r(x', x) = \frac{d\Omega_x}{dA_{x'}}. \tag{2.12}$$

$\Delta_r(x', x)$ is the ratio between the angular opening of a pencil of rays at the point x and the area spanned at the final point x' following the path r. For $N = 3$ we have

$$G_r(x', x, k) = (-1)^{n_r} \frac{\Delta_r^{1/2}(x', x)}{4\pi} e^{ik\square_r(x', x)}. \tag{2.13}$$

With this explicit form for the propagator G, we now have to rewrite the elements of the quadratic operator $T_{\mu\nu}$ as functions of G and its derivatives. It is useful to pass from the point-splitting to a frequency cutoff by inserting the latter in the normal modes decomposition (2.6) as

$$e^{-k_j/\Lambda} = \int_0^\infty dk\, e^{-k/\Lambda} 2k\delta\left(k^2 - k_j^2\right). \tag{2.14}$$

The limit $x' \to x$ can then be exchanged with the dk integral and we get for the energy density,

$$\langle 0|T_{00}(x, t)|0\rangle = \int_0^\infty dk\, e^{-k/\Lambda} \frac{1}{2} E(k)\rho(x, k) + \int_0^\infty dk\, e^{-k/\Lambda} \frac{k}{2E(k)} \vec{\nabla} \cdot \vec{j}(x, k). \tag{2.15}$$

The density ρ and the vector $\vec{j}$ are defined as

$$\rho(x, k) = \frac{2k}{\pi} \operatorname{Im} G(x, x, k), \tag{2.16}$$

$$\vec{j}(x,k) = \lim_{x'\to x} \frac{1}{\pi} \operatorname{Im} \vec{\nabla} G(x',x,k) = \frac{1}{2\pi} \operatorname{Im} \vec{\nabla} G(x,x,k). \tag{2.17}$$

$\mathcal{E}$ is obtained by integrating T_{00} over the whole volume between the bodies:

$$\mathcal{E} = \int_{\mathcal{D}} d^3x \int_0^\infty dk\, e^{-k/\Lambda} \frac{1}{2} E(k) \rho(x,k) + \int_0^\infty dk\, e^{-k/\Lambda} \frac{k}{2E(k)} \int_{\mathcal{S}} d\vec{S} \cdot \vec{j}(x,k). \tag{2.18}$$

We have turned the integral over the divergence of $\vec{j}$ into a surface integral using Gauss's theorem. In the case of Dirichlet or Neumann boundary conditions, since $d\vec{S} \propto \vec{n}$ we have (here $\partial_{\vec{n}} \quad \vec{n}\cdot\vec{\nabla}$ and $j_{\vec{n}} = \vec{n}\cdot\vec{j}$)

$$j_{\vec{n}}(x,k) = \frac{1}{\pi} \operatorname{Im} \partial_{\vec{n}} G(x,x,k) = 0, \quad x \in \mathcal{S} \tag{2.19}$$

and the surface integral term disappears. It should be noted that the vanishing of the $\vec{j}$ contribution to the total energy relies on the continuity of the propagator for $x', x \in \mathcal{D}$. In some approximations, including the optical one, this continuity is lost. Hence spurious surface terms arise on the boundary of certain domains $\mathcal{D}' \quad \mathcal{D}$. This region is what in wave optics is called the 'penumbra' region. Diffractive contributions are also not negligible in this region and they cancel the discontinuities in G, hence eliminating the surface terms.[1] The surface terms in the energy are hence of the same order of the diffractive contributions which define the error in our approximation.

The divergence $\vec{\nabla}\cdot\vec{j}$ could also be eliminated from T_{00} by changing the energy–momentum tensor according to

$$\tilde{T}_{\mu\nu} = T_{\mu\nu} + \partial^\alpha \psi_{\alpha\mu\nu}, \tag{2.20}$$

with

$$\psi_{\alpha\mu\nu} = \frac{1}{2}\varphi(g_{\mu\nu}\partial_\alpha - g_{\alpha\nu}\partial_\mu)\varphi. \tag{2.21}$$

The total energy $\mathcal{E}$ and momentum are not affected by this redefinition however the new tensor $T_{\mu\nu}$ is not symmetric.

It can be seen that the stress tensor T_{ij} is normal on the surface $\mathcal{S}$ (for both Dirichlet and Neumann BC) so locally the force on the surface is given by the pressure alone

$$\frac{d\vec{F}}{dS} = \vec{n}P = \langle 0|T_{\vec{n},\vec{n}}|0\rangle. \tag{2.22}$$

The operator $T_{\vec{n}\vec{n}}$ regulated by point splitting is

$$\begin{aligned} T_{\vec{n},\vec{n}}(x,t) &= \lim_{x'\to x}\left[\partial'_{\vec{n}}\varphi'\partial_{\vec{n}}\varphi - \frac{1}{2}g_{\vec{n},\vec{n}}\left(\partial'_0\varphi'\partial_0\varphi - \vec{\nabla}'\varphi'\cdot\vec{\nabla}\varphi - m^2\varphi^2\right)\right] \\ &= \lim_{x'\to x}\left[\partial'_{\vec{n}}\varphi'\partial_{\vec{n}}\varphi + \frac{1}{2}\left(\partial'_0\varphi'\partial_0\varphi + \varphi'\vec{\nabla}^2\varphi - m^2\varphi^2\right) - \frac{1}{2}(\vec{\nabla}' + \vec{\nabla})\varphi'\vec{\nabla}\varphi\right] \end{aligned} \tag{2.23}$$

where φ' is shorthand for $\varphi(x',t)$. The second term in brackets is zero when averaged over an eigenstate of the number operator $|\{n_j\}\rangle$, by virtue of the equations of motion. For Dirichlet BC

[1] As an example see Kirchoff's treatment of the diffraction from a hole in Ref. [19].

the term $\varphi\vec{\nabla}^2\varphi = 0$ on the boundaries, so we have ($\vec{\nabla} = \vec{n}\partial_{\vec{n}} + \vec{\nabla}_t$)

$$\langle 0|T_{\vec{n},\vec{n}}|0\rangle = \lim_{x'\to x}\sum_j \frac{1}{4E_j}\left(\partial'_{\vec{n}}\partial_{\vec{n}} - \vec{\nabla}'_t\cdot\vec{\nabla}_t + k_j^2\right)\psi_j(x')\psi_j(x). \tag{2.24}$$

Since also $\vec{\nabla}_t\psi_j(x) = 0$ on the boundaries this expression simplifies to

$$P(x) = \lim_{x'\to x}\sum_j \frac{1}{4E_j}\partial'_{\vec{n}}\partial_{\vec{n}}\psi_j(x')\psi_j(x). \tag{2.25}$$

This expression can be rewritten, in terms of the propagator G, regulated by a frequency cutoff as we did for T_{00},

$$P(x) = \lim_{x'\to x}\partial'_{\vec{n}}\partial_{\vec{n}}\int_0^\infty dk\, e^{-k/\Lambda}\frac{k}{2\pi E(k)}\operatorname{Im} G(x',x,k). \tag{2.26}$$

In this regulated expression we can exchange the derivatives, limit and integral safely. Below we discuss what the divergences are when $\Lambda\to\infty$ and how to interpret and dispose them.

All the above expressions are exact. Once the propagator G is known, we can calculate the energy–momentum tensor components from them. However as discussed above in the interesting cases it is difficult to find an exact expression for G and some approximations must be used.

For smooth impenetrable bodies we use the optical approximation to the propagator developed in Refs. [10,11] and recalled in Eq. (2.11). This gives G as a series of optical paths and hence the pressure P as a sum of contributions due to optical paths which reflect over the smooth, metallic surfaces[2]

$$P \simeq \sum_r P_r, \tag{2.27}$$

$$P_r = (-1)^{n_r}\lim_{x'\to x}\partial'_{\vec{n}}\partial_{\vec{n}}\int_0^\infty dk\, e^{-k/\Lambda}\frac{k}{2\pi E(k)}\frac{\Delta_r^{1/2}(x',x)}{4\pi}\sin\left(k\square_r(x',x)\right). \tag{2.28}$$

An important feature of the optical approximation is that all divergences are isolated in the low reflection terms whose classical path length can vanish as $x', x\to\mathcal{S}$. In practice only the zeroth and first reflection are potentially divergent. Before performing the integral in k and taking $\Lambda\to\infty$ then we have to put aside the divergent zero and one reflection terms P_0 and P_1 for a moment (in the next section we will show how their contributions are to be interpreted).

For the remaining families of paths (that we will denote as $r\in\mathcal{R}$) the integral over k can be done and the limit $\Lambda\to\infty$ taken safely. The result is finite and reads

$$P(x) = \sum_{r\in\mathcal{R}}\lim_{x'\to x}\partial'_{\vec{n}}\partial_{\vec{n}}(-1)^{n_r}\frac{\Delta_r^{1/2}(x',x)}{8\pi^2\square_r(x',x)}. \tag{2.29}$$

[2] If the conducting surfaces are rough and the average height h of the roughness is much smaller than the important wavelengths a, then the surfaces can be considered, for what we are concerned, smooth [12]. The corrections to the Casimir energy in the optical approximation are still not known but they must be very small, $\mathcal{O}(\langle h^2\rangle)$ since $\langle h\rangle = 0$ the average being on regions of size a.

We can further simplify this expression. For simplicity let us call z the normal direction. Notice that for any sufficiently smooth function $f(z', z)$ vanishing for either z' or z on the surface $z = 0$

$$\partial_{z'}\partial_z f(z', z)\big|_{z'=z=0} = \frac{1}{2}\partial_z^2 f(z, z)\big|_{z=0}. \tag{2.30}$$

The proof is trivial: consider that the lowest order term in the expansion of $f(z', z)$ near $z', z = 0$ is $\propto z'z$. The propagator $G(x', x, k)$ satisfies all these properties and hence we can use this result to get rid of the limit $x' \to x$ and assume $x' = x$ from the beginning. We can therefore rewrite Eq. (2.29) as,

$$P(x) = \sum_{r\in\mathcal{R}} (-1)^{n_r} \partial_z^2 \frac{\Delta_r^{1/2}(x, x)}{16\pi^2 \square_r(x, x)}. \tag{2.31}$$

Eq. (2.31) is one of the main results of this paper. In Ref. [11] we reduced the computation of Casimir energy to a volume integral. The force is then found by taking the derivative with respect to the distance between the bodies. Calculating the pressure instead gives the force by means of just a double integral of a local function. The problem is then computationally lighter and sometimes (as we will see in the examples) can even lead to analytic results.

Essentially the problem has been reduced to finding the lengths and enlargement factors associated with the optical paths *for points close to the boundary*. In the case of the pressure (Eq. (2.29) or (2.31)) it is necessary to know their derivatives in the direction transverse to the surfaces. We will see that this problem can be easily tackled numerically when it cannot be solved analytically.

2.2. Regulate and eliminate divergences

As in the energy calculations [11], the only divergences occurring in the pressure come from by paths whose lengths $\square \quad 1/\Lambda$, where Λ is the plasma frequency of the material.[3] There are only two such families of paths: the zero and one reflection paths. In this section we show that these divergent contributions are independent of the distances between the bodies. This fact is easily understood: in order for a path to have arbitrarily small length all of its points must be on the same body. So in order to study these terms we need only consider a single, isolated body (and a massless field). We are also careful in maintaining the double derivative $\partial^2_{z',z}$ since we are calculating the terms P_0 and P_1 separately.

For $r = 0$, the zero reflection term, introducing an exponential cutoff Λ on the material reflection coefficient we obtain

$$P_0 = \int_0^\infty e^{-k/\Lambda}\, dk \frac{k}{2\pi E(k)} \lim_{x'\to x\in\mathcal{S}} \partial_{z'}\partial_z \left(\frac{\sin k|z' - z|}{4\pi|z' - z|}\right) = \frac{\Lambda^4}{4\pi^2}. \tag{2.32}$$

[3] It is well known that the forces between rigid bodies remain finite and do not depend on the characteristics of the material in the perfect metal limit. On the contrary, stresses on the isolated bodies are strongly dependent on the dielectric constants and in general diverge in the perfect metal limit [17]. However, in the case of finite dielectric constants the calculation of the Casimir force is possible only in the parallel plates case [18]: a description of the interplay of finite conductivity effects and geometry dependence, even within the optical approximation, is still lacking. So in this paper we limit ourselves to the case of infinite conductivity (which is however a very good approximation for the experiments) and we neglect the infinite self-stresses induced by this idealization.

The same calculation for the $r = 1$ or one reflection term gives:

$$P_1 = \int_0^\infty e^{-k/\Lambda}\, dk \frac{k}{2\pi E(k)} \lim_{x' \to x \in \mathcal{S}} \partial_{z'}\partial_z \left(-\frac{\sin k|z'+z|}{4\pi|z'+z|} \right) = \frac{\Lambda^4}{4\pi^2}. \tag{2.33}$$

Notice that these two terms are equal, so we could have substituted $\partial_{z',z} \to \frac{1}{2}\partial_z^2$ for their sum, after having properly regulated the divergence.

This positive, cutoff dependent pressure, $P_\Lambda \quad P_0 + P_1$, must be dynamically balanced locally by a pressure generated by the material, lest it collapse. Moreover the total force obtained by integrating this quantity over the (closed) surface $\mathcal{S}$ of the whole body gives zero. However, if the space around the body were inhomogeneous, as in the presence of a gravitational field, a finite term survives the surface integration, giving rise to a "vacuum Archimedes effect" in which the pressure on one side is, due to gravitational effects, larger than on the other side, so the body feels a net force. We have analyzed this effect in detail in Ref. [20] and called it "Casimir buoyancy".

Finally note that another important element of this class of quadratic operators is the Feynman propagator. In studying a field theory in a cavity or in between impenetrable bodies (for example, hadrons as bags, photons in cavities or Bose–Einstein condensates in traps), we can consider expanding the Feynman propagator in a series of classical optical paths reflecting off the boundaries. The first term, related to the direct path is the familiar free propagator, the others give the finite volume corrections.

3. Examples

In this section we calculate the Casimir force from the pressure, using the formalism developed in the previous section, for three examples that were already addressed in Ref. [11] using the energy method.

3.1. Parallel plates

The parallel plates calculation is a classic example, whose result is well known and constitutes the basis the widely used proximity force approximation (PFA) [16]. We use this standard example to establish the rank among contributions to the total pressure and show the similarity and differences with the energy method [11].

We calculate the force acting on the lower plate, denoted by d or *down*, by calculating the pressure on its surface. We discard the zero and $1d$ (one reflection on the lower plate itself) reflection terms. The first term to be considered is the path that bounces once on the upper plate (u or *up*) $1u$. For parallel plates $\Delta = 1/\square^2$ and we have

$$P(x) = \sum_{r \geqslant 1u} (-1)^{n_r} \partial_z^2 \frac{1}{16\pi^2 \square_r^2(x,x)}. \tag{3.1}$$

The length $\square_r(x,x)$ for the paths that bounce an even number of times is a constant in z and hence the derivatives vanish: they do not contribute to the pressure. This seemingly innocuous observation simplifies the calculations considerably and it is a test for any other geometry which reduces to parallel plates in some limit: in this limit the even reflections contributions must vanish. Generically their contributions are small. This parallels the role of the odd reflection paths in the energy method [11].

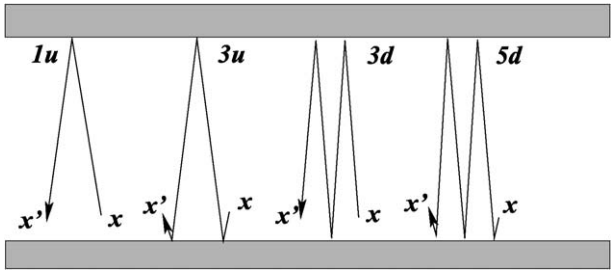

Fig. 1. Odd reflection paths that contribute to the Casimir force between the two plates in the pressure calculations with the optical approximation. The points x' and x will eventually be taken coincident and lying on the lower plate.

Fig. 1 shows the odd reflection paths labelled with our conventions. For the path 1u we have

$$P_{1u}(x) = \lim_{z\to 0} -\partial_z^2 \frac{1}{16\pi^2(2a-2z)^2} = -\frac{3}{32\pi^2 a^4}. \tag{3.2}$$

The next path to be considered is the path that bounces 3 times, first on d, then on u and again on d, dud = 3u (3 stands for 3 reflections and u for the plate where the middle reflection occurs) which gives a contribution

$$P_{3u}(x) = \lim_{z\to 0} -\partial_z^2 \frac{1}{16\pi^2(2a+2z)^2} = -\frac{3}{32\pi^2 a^4}. \tag{3.3}$$

The two contributions Eqs. (3.2) and (3.3) are equal. The reason is easily uncovered. One can recover Eq. (3.3) from Eq. (3.2) sending $z \to -z$ but for the purpose of taking the second derivative at $z = 0$ this is irrelevant. In the same fashion $P_{3d} = P_{5d}$, $P_{5u} = P_{7u}$, etc., and hence we find

$$P(x) = -2\frac{3}{32\pi^2 a^4} - 2\frac{3}{32\pi^2(2a)^4} - 2\frac{3}{32\pi^2(3a)^4} + \cdots = -\frac{3}{16\pi^2 a^4}\frac{\pi^4}{90}, \tag{3.4}$$

which is the well-known result. Notice also that the rate of convergence is the same as in the calculation making use of the Casimir energy in Ref. [11] (nth term contributes $1/n^4$ of the first term, in this case 1u + 3u). These observations that allow us to determine the rank of the contributions are fundamental, and they apply as well to the other examples in this section.

3.2. The Casimir torsion pendulum

In this section we study a geometry already considered in Ref. [11]: a plate inclined at an angle θ above another infinite plate. We have called this configuration a 'Casimir torsion pendulum' because the Casimir force will generate a torque which can be experimentally measured. The configuration is analogous to the parallel plates case but the upper plate must be considered tilted at an angle θ from the horizontal. The length of the upper plate must be taken finite, we denote it by w, while the length of the lower plate can be infinite which we choose for simplicity. There is only one substantial difference with the parallel plates case: the even reflection paths do contribute in the pendulum, since their length varies as we move the final points x', x.

We calculate the force exerted on the lower, infinite plate for simplicity. We then obtain the energy $\mathcal{E}$, by integrating over the distance along the normal to the lower plate and from this we

can calculate the torque as

$$\mathcal{T} = -\frac{\partial \mathcal{E}}{\partial \theta}. \tag{3.5}$$

The lower plate is taken infinite, the upper plate width is w, and the distance between the height at the midpoint of the upper plate is a. We will choose as the origin of the coordinates one point on the intersection line between the lower plate and the line obtained by prolonging the upper plate. This defines a fictitious wedge of opening angle θ. We call x the horizontal and z the vertical coordinate, the third direction, along which one has translational symmetry, being y.

Since the surfaces are locally flat we have $\Delta = 1/\square^2$ as in the case of the parallel plates, and again the odd reflections are exactly as in the case of the parallel plates. However now the even reflections contribute (the notation is the same as in the parallel plates case, in the even reflections $2u$ means the first reflection is on the upper plate, etc.):

$$P = P_{1u+3u} + P_{2u+2d} + P_{3d+5d} + \cdots, \tag{3.6}$$

where we have grouped the terms with the symbolic notation $P_{a+b} = P_a + P_b$ when $P_a = P_b$. It is useful to recapitulate what we have learned about the rank of these contributions: P_{1u+3u} dominates, P_{3d+5d} is smaller by $1/16$, P_{5u+7u} is smaller by $1/81$, etc. The even reflections are generically much smaller than the odd reflections, and vanish as $\theta \to 0$.

The first term in (3.6) is

$$P_{1u+3u} = -2\frac{1}{16\pi^2}\partial_z^2 \frac{1}{\square_1^2(z,x)}, \tag{3.7}$$

with $\square_1 = 2(x\sin\theta - z/\cos\theta)$, and an overall factor of 2 takes into account the identity $P_{1u} = P_{3u}$. Taking the derivative and then setting $z = 0$ we find

$$P_{1u+3u} = -\frac{3}{16\pi^2}\frac{1}{x^4\sin^4\theta\cos^2\theta}, \tag{3.8}$$

and integrating from $x_m = (a/\sin\theta - w/2)/\cos\theta$ to $x_M = (a/\sin\theta + w/2)/\cos\theta$ we find the force per unit length in the y direction

$$F_{1u+3u} = -\frac{\cos\theta}{32\pi^2\sin^4\theta}\left(\frac{1}{(a/\sin\theta - w/2)^2} - \frac{1}{(a/\sin\theta + w/2)^2}\right). \tag{3.9}$$

Since term by term $F = -\partial\mathcal{E}/\partial a$ we find the first term in optical expansion of the Casimir energy $\mathcal{E}$ (the arbitrary constant is chosen so that $\mathcal{E} \to 0$ when $a \to \infty$) as

$$\mathcal{E}_{1u+3u} = -\frac{aw\cos^4\theta}{2\pi^2(4a^2 - w^2\sin^2\theta)^2} \tag{3.10}$$

and from this one obtains the torque

$$\mathcal{T}_{1u+3u} = \frac{2aw(w^2 - 4a^2)\cos^3\theta\sin\theta}{\pi^2(4a^2 - w^2\sin^2\theta)^3}. \tag{3.11}$$

Analogously we can calculate the contribution to the pressure P of the two reflections paths $2u$ and $2d$. Again the contributions of the two paths are identical and the result simplifies to

$$P_{2u+2d} = \frac{2}{8\pi^2}\frac{1}{2}\partial_z^2 \frac{1}{\square_2^2(z,x)}, \tag{3.12}$$

and using $\ell_2 = 2\sqrt{x^2+z^2}\sin\theta$ we find

$$P_{2u+2d} = -\frac{1}{16\pi^2 \sin^2\theta\, x^4} \tag{3.13}$$

which integrated from $x_m = (a/\sin\theta - w/2)/\cos\theta$ and $x_M = (a/\sin\theta + w/2)/\cos\theta$ gives the force along the z axis due to these paths:

$$F_{2u+2d} = -\frac{\cos^3\theta}{48\pi^2\sin^2\theta}\left(\frac{1}{(a/\sin\theta - w/2)^3} - \frac{1}{(a/\sin\theta + w/2)^3}\right). \tag{3.14}$$

This expression can now be expanded for $\theta \ll 1$ (quasi-parallel plates)

$$F_{2u+2d} \simeq -\frac{1}{16\pi^2}\left(\frac{w}{a^4}\theta^2 + \frac{5w^3 - 11wa^2}{6a^6}\theta^4 + \cdots\right). \tag{3.15}$$

Notice that this expression vanishes when $\theta \to 0$, as it should since for parallel plates all the contributions of even reflections paths vanish.

The next term in the series is F_{3d+5d}, whose calculation is performed in the same fashion. The result is:

$$F_{3d+5d} = -\frac{3}{16\pi^2}\frac{\cos^5 2\theta}{\sin^4 2\theta}\left(\frac{1}{(a/\sin\theta - w/2)^3} - \frac{1}{(a/\sin\theta + w/2)^3}\right), \tag{3.16}$$

$$\simeq -\frac{1}{16\pi^2}\left(\frac{3w}{16a^4} + \frac{5w^3 - 48a^2w}{32a^6}\theta^2 + \cdots\right). \tag{3.17}$$

We can also present the term given by the 4 reflections paths,

$$F_{4u+4d} = -\frac{\cos^3 2\theta}{48\pi^2\sin^2 2\theta}\left(\frac{1}{(a/\sin\theta - w/2)^3} - \frac{1}{(a/\sin\theta + w/2)^3}\right)$$

$$\simeq -\frac{1}{16\pi^2}\left(\frac{w}{4a^4}\theta^2 + \cdots\right). \tag{3.18}$$

The terms independent of θ can be seen to reconstruct the parallel limit case $F = -(1 + 1/16 + 1/81 + \cdots)3/16\pi^2 a^4$.

Term by term, this series for the force reproduces the series in Ref. [11]. The series for the energy and the torque agree as well. The results of the pressure method then coincide with those of the energy method (as for all the examples analyzed in this paper). In Ref. [11] we discussed at some length the predictions of the optical method for the Casimir torsion pendulum. We will not repeat them here, referring the reader to that paper for further details.

3.3. Sphere and plane

The sphere facing a plane is an important example for several reasons: it has been analyzed theoretically with various exact or approximate numerical techniques [8,21]; it is an experimentally relevant configuration; the exact solution is unknown and probably will escape analytical methods for a long time to come. We have already calculated the optical approximation to the Casimir energy in Ref. [11] up to 5 reflections. In this paper we study this problem for mainly pedagogical purposes, leaving a more accurate and complete numerical analysis for the future. We believe it is worth studying this example because, contrary to the previous two examples,

the enlargement factor plays an important role and moreover we will reanalyze this example with finite temperature in Section 4.2.1.

We calculate the pressure (and by integrating, the force) exerted on the plate by the sphere which, of course, equals the force exerted by the plate on the sphere. We start from the qualitative observation that the rank of the contributions is the same as in the parallel plates case in the limit $a/R \to 0$. In all the examples we have analyzed this rank is preserved for any value of a/R. Moreover the ratios of the contributions to the force $F_{3+5}(a,R)/F_{1+3}(a,R)$, $F_4(a,R)/F_2(a,R)$, etc., decrease quickly as a/R increases, we believe due to the growing importance of the enlargement factor.

In this paper we calculate analytically the 1s term (here s stands for 'sphere' and p for 'plate') and by using the relation P_{1s+3s} $P_{1s}+P_{3s}=2P_{1s}$ proved in Section 2 (the notation is the same as in that section) we are able to include the 3s term as well.

Using the expressions for the length and enlargement factor for the 1s path obtained in Ref. [11] we get

$$\begin{aligned} P_{1s+3s} &= -2\frac{R}{16\pi^2}\frac{\partial^2}{\partial z^2}\frac{\Delta_{1s}^{1/2}}{\square_{1s}} \\ &= -\frac{R}{32\pi^2}\frac{\partial^2}{\partial z^2}\Big(R-\sqrt{(a+R-z)^2+\rho^2}\Big)^{-2}\big((a+R-z)^2+\rho^2\big)^{-1/2}\big|_{z=0}. \end{aligned} \tag{3.19}$$

The final expression for the pressure P_{1s+3s} obtained after the derivatives are taken is rather long, however the contribution to the force on the plate, F_{1s+3s} (obtained by integration of P_{1s+3s} over the infinite plate) is quite simple:

$$F_{1s+3s} = 2\pi\int_0^\infty d\rho\,\rho P_{1s+3s} = -\frac{\hbar c R}{8\pi a^3}. \tag{3.20}$$

This is the largest of the contributions and increasing a/R improves the convergence of the series due to the presence of the enlargement factor, so the asymptotic behavior at large a/R predicted by the optical approximation is that given by this formula, i.e. $F \propto R/a^3$ or $E \propto R/a^2$. This asymptotic law is in accordance with the numerics of Ref. [10] and the predictions of other semiclassical methods [21]. However, Eq. (3.20) is in disagreement with the Casimir–Polder law [24] which predicts $E \propto R^3/a^4$ for $a \ll R$. This is no great surprise, since our method is not valid for $a/R \ll 1$, the semiclassical reflections being corrected and eventually overshadowed by diffractive contributions [22,23].

We have calculated the contribution of the two reflections paths analytically as well. The calculation is more involved than the one reflection term but a big simplification occurs if one notices that, for the purpose of taking the second derivative with respect to z at $z=0$, one can leave the reflection point on the sphere fixed. We could not prove a similar result for any other reflection. It is certainly not true for *odd* reflections but one can conjecture it to be true for *even* reflections. In this paper we have not calculated the 4 reflection terms and hence we could not check this conjecture for more than 2 reflections.

And finally, we have calculated the 3p (or sps) and hence obtained the 5p, or pspsp, paths contribution P_{3p+5p}; P_{3p+5p} in the parallel plates limit should account for $1/16$ of the total force. This contribution, unlike the previous ones, must be calculated partly numerically, mainly

because finding the reflection point on the sphere requires the (unique) solution of a transcendental equation. This task is achieved much more quickly by a numerical algorithm than by patching together the several branches of the analytic solution.

The total pressure is plotted in Fig. 2 while the various contributions (keeping in mind that P_{1s+3s} and P_{3p+5p} are negative and P_{2+2} is mainly positive) are shown in Fig. 3. Fig. 2 reveals some interesting features of the pressure in this geometry: the total pressure decays very quickly with the distance as $P \quad \rho^{-\alpha}$: the exponent α seems to depend upon the distance a/R, but for $a/R \leqslant 0.1$ a good fit is obtained with $\alpha = 6$, in accordance with the asymptotic expansion of the $1 + 3$ reflection term Eq. (3.19); by decreasing the distance between the sphere and the plate, the pressure becomes more and more concentrated near the tip, giving us reasons to trust our approximation and supporting the use of the PFA as a first approximation in the limit $a/R \to 0$. Fig. 3 shows the relative importance of the contributions due to the different paths. As expected the contribution to the total pressure decreases quite fast by increasing the number of reflections. In Fig. 4 one can also see that the sign of the pressure is not determined simply by the number of reflections of the underlying optical path—as for the contribution to the energy density.

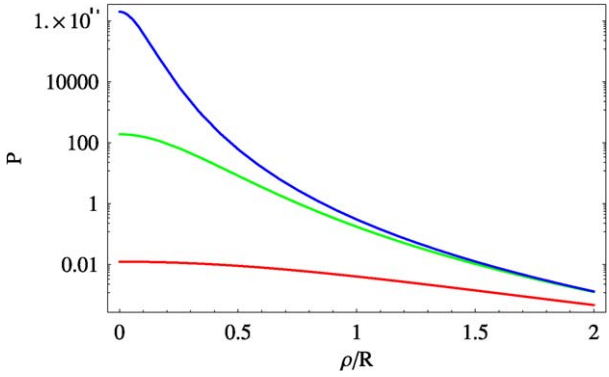

Fig. 2. (Colour online.) The magnitude of the total pressure up to reflection $5p$ in units of $\hbar c/R^4$ as a function of the radial coordinate on the plate, ρ/R. Upward, or red to blue $a/R = 1$, $a/R = 0.1$ and $a/R = 0.01$.

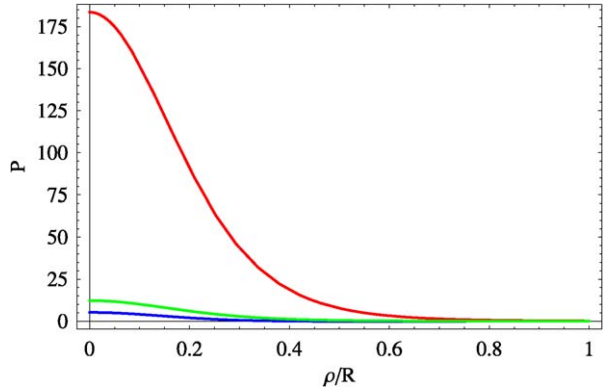

Fig. 3. (Colour online.) Contributions to the pressure in units of $\hbar c/R^4$ as a function of ρ/R, for fixed $a/R = 0.1$. Downward or red to blue, we have $-P_{1s+3s}$, $-P_{3p+5p}$ and P_{2+2}. Although unnoticeable in this figure, the curve P_{2+2} changes sign at around $\rho/R \simeq 0.4$ (see Fig. 4 for a similar situation).

By integrating the pressure over the whole plate we obtain the force F. It is useful to factor out the most divergent term of the force, as predicted by the PFA, so we define the quantity $f(a/R)$ as

$$F(a) = -\frac{\pi^3 R}{720 a^3} f(a/R). \tag{3.21}$$

Since we include only a finite number of reflections it is convenient to factor out the constant $\zeta(4)/(1+1/16)$ such that f is normalized with $f(0) = 1$. The function $f(a/R)$, calculated including paths $1s$, $3s$, 2, $3p$ and $5p$, is plotted in Fig. 5. When $a/R \to 0$ f is fitted by

$$f(a/R) = 1 - 0.10 a/R + \mathcal{O}\big((a/R)^2\big). \tag{3.22}$$

By comparing to the results of [10]

$$f_{\text{energy}}(a/R) = 1 + 0.05 a/R + \mathcal{O}\big((a/R)^2\big) \tag{3.23}$$

there is the difference in the subleading term.

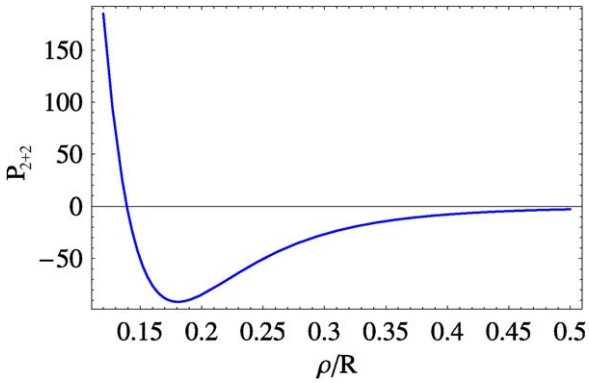

Fig. 4. Contribution of the two reflection path(s) to the pressure in units of hc/R^4 as a function of ρ/R, for fixed $a/R = 0.01$. The pressure becomes negative, showing that the sign of the pressure is not determined by the number of reflection only.

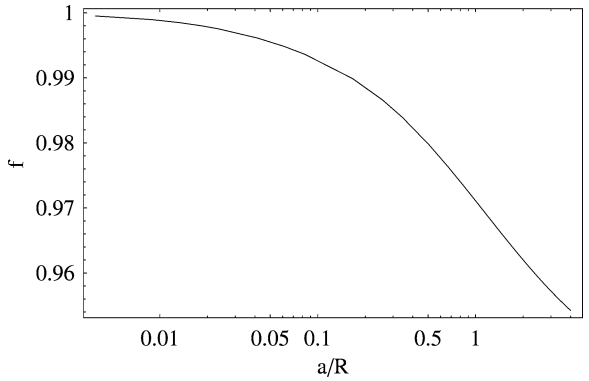

Fig. 5. The ratio between the optical force up to the $5p$ reflection and the most divergent term in the PFA, as defined by Eq. (3.21).

By neglecting the $5s + 7p$ reflection paths (which in the parallel plates case contribute 2% of the total force) we can only assert that the functions f in (3.22) and (3.23) represent the optical approximation with an error of 2%. When plotted on the whole range of a/R where the optical approximation is to be trusted the pressure and energy method curves never differ more than 2%. However there is no such a bound on the subleading term which, on the contrary, depends on the higher reflections contributions which have not been included in this calculations.[4] With the terms calculated at this point, we cannot make a precise statement about the subleading term. We can however safely say that the subleading term a/R coefficient is quite small and our method disagrees with the PFA prediction $-0.5a/R$. The sphere opposite plate is such an experimentally relevant geometry that further, more accurate studies need to be performed to compare with experimental data.

In conclusion, the lessons to be learned from this example are two: (1) The calculations with the pressure method are even quicker and simpler than the energy method and sometimes can give analytic results for non-trivial geometries and (2) the subleading terms must be compared only between calculations performed with the same accuracy.[5]

4. Casimir thermodynamics

As measurements of Casimir forces increase in accuracy they become sensitive to thermal effects. The natural scale for Casimir thermodynamics is a distance, $\tilde{\beta} = \hbar c/\pi T$, which at room temperature is about 2.5 microns. (To avoid confusion with the wave number k, we set Boltzmann's constant equal to unity and measure temperature in units of energy. We continue to keep $\hbar$ and c explicit.) So, assuming the corrections are of $\mathcal{O}((a/\tilde{\beta})^{\alpha})$, depending on the value of α thermal effects might be expected between the 10% (for $\alpha = 1$) and 0.3% (for $\alpha = 4$, the standard parallel plates result) level for Casimir force measurements on the micron scale. In open geometries, like the sphere and plane, even longer distance scales are probed by Casimir effects, and this gives rise to interesting changes in the temperature dependence of the Casimir free energy in comparison with the case of parallel plates [3]. The optical approximation is well suited for discussion of thermodynamics since the thermodynamic observables, like the Casimir energy, can be expressed in terms of the propagator. Here we consider again a non-interacting, scalar field outside rigid bodies on which it obeys Dirichlet boundary conditions.

Before entering into a technical discussion of temperature effects, it is useful to anticipate one of our central results which follows from qualitative observations alone. As $T \to 0$ the temperature effects probe ever longer distances. Even at room temperature the natural thermal scale is an order of magnitude larger than the separation between the surfaces in present experiments (see Ref. [5]). Since long paths contribute little to the Casimir force, we can be confident that thermal effects vanish quickly at low temperature. However, the leading T-dependence at small T comes from regions beyond the range of validity of the optical (or any other) approximation, so we are

[4] For example, consider that including only $1s, 3p$, and 2 and reflections would have given a subleading term $-0.16a/R$ instead of $-0.10a/R$ in Eq. (3.22). The subleading term then changes of 50% by adding the $3s + 5p$ reflection terms which contributes only up to 8% of the total.

[5] A.S. would like to thank M. Schaden and S. Fulling for conversations on this point during the workshop 'Semiclassical approximations to vacuum energy' held at Texas A & M, College Station, TX, January 2005. The concerns about the errors to be associated with the optical, semiclassical or proximity force approximation is still open to debate and is strictly connected to one of the most challenging open problems in spectral theory i.e. how to go beyond the semiclassical approximation to the density of states of a positive Hermitian operator.

unable to say definitively how they vanish for geometries where no exact solution is possible (i.e. other than infinite parallel plates).

This section is organized as follows: First we discuss the free energy and check our methods on the parallel plates geometry; then we discuss the temperature dependence of the pressure, which we apply to the sphere and plate case. Finally we discuss the difficulties associated with the $T \to 0$ limit.

4.1. Free energy

The free energy is all one needs to calculate both thermodynamic corrections to the Casimir force and Casimir contributions to thermodynamic properties like the specific heat and pressure. However like the Casimir *energy*, Casimir contributions to the specific heat, pressure, etc., are cutoff dependent and cannot be defined (or measured) independent of the materials which make up the full system. So we confine ourselves here to the thermal corrections to the Casimir force. The problem of parallel plates has been addressed before and our results agree with those [3].

4.1.1. Derivation

We start from the expression of the free energy for the scalar field as a sum over modes

$$\begin{aligned}\mathcal{F}_{\text{tot}} &= -\beta^{-1}\sum_n \ln\left(\frac{e^{-\beta\frac{1}{2}\hbar\omega_n}}{1-e^{-\beta(\omega_n-\mu)}}\right),\\ &= \beta^{-1}\sum_n \ln\left(1-e^{-\beta(\hbar\omega_n-\mu)}\right)+\sum_n\frac{1}{2}\hbar\omega_n,\\ &\mathcal{F}+\mathcal{E},\end{aligned} \tag{4.1}$$

where μ is the chemical potential, and the last term is the Casimir energy, or the free energy at zero temperature, since $\mathcal{F}=0$ for $T=0$. The Casimir energy $\mathcal{E}$, being independent of the temperature, does not contribute to the thermodynamic properties of the system. It however does contribute to the pressures and forces between two bodies. The force between two bodies, say a and b, is obtained by taking the gradient of the free energy with respect to the relative distance $\vec{r}_{ab}$

$$\vec{f}_{ab} = -\vec{\nabla}_{ab}\mathcal{F}. \tag{4.2}$$

At $T=0$ we recover the familiar result $\vec{f}=-\vec{\nabla}\mathcal{E}$.

Next we turn the sum over modes into a sum over optical paths. Following the same steps that led from Eq. (2.4) to Eq. (2.15) we obtain

$$\mathcal{F} = \beta^{-1}\int d^N x\int_0^\infty dk\,\rho(x,k)\ln\left(1-e^{-\beta(\hbar\omega(k)-\mu)}\right), \tag{4.3}$$

where $\rho(x,k)$ is given by Eq. (2.16). By specializing to a massless field in 3 dimensions with zero chemical potential (to mimic the photon field), and substituting the optical approximation for the propagator Eq. (2.13), we obtain the sum over paths

$$\mathcal{F}\quad \sum_{r=0}\mathcal{F}_r = \sum_r(-1)^r\frac{1}{2\pi^2\beta}\int_{\mathcal{D}_r} d^3x\,\Delta_r^{1/2}\int_0^\infty dk\,k\sin(k\square_r)\ln\left(1-e^{-\beta\hbar ck}\right). \tag{4.4}$$

Here the term $\mathcal{F}_0$, the direct path, gives the usual free energy for scalar black body radiation. Using the values for the direct path, we have $\Delta_0 = 1/\ell_0^2$ and $\ell_0 = |x' - x| \to 0$ when taking $x' \to x$. We get the familiar textbook expression

$$\mathcal{F}_0 = V \int_0^\infty dk \frac{k^2}{2\pi^2} \beta^{-1} \ln\left(1 - e^{-\beta\hbar c k}\right) = -\frac{\pi^2}{90} \frac{V T^4}{(\hbar c)^3}, \tag{4.5}$$

where V is the (possibly infinite) volume outside the bodies.

The general term $\mathcal{F}_r$ associated with the path r is calculated by performing the k integral in Eq. (4.4):

$$\mathcal{F}_r = (-1)^{r+1} \frac{\hbar c}{2\pi^2} \int_{\mathcal{D}_r} d^3x \, \Delta_r^{1/2} \frac{1}{2\ell_r^3} \left[-2 + \tilde{\ell}_r \left(\coth \tilde{\ell}_r + \tilde{\ell}_r \operatorname{csch}^2 \tilde{\ell}_r\right)\right] \tag{4.6}$$

where $\tilde{\ell}_r = \ell_r \pi T/\hbar c = \ell_r/\tilde{\beta}$ measures the path length relative to the thermal length scale.

Eq. (4.6) is the fundamental result of this section and gives a simple, approximate description of thermal Casimir effects for geometries where diffraction is not too important. There are no divergences in any of the $\mathcal{F}_r$, ultraviolet or otherwise, even for the direct path (as we saw in Eq. (4.5)) and the first reflection path. All the ultraviolet divergences are contained in the Casimir energy $\mathcal{E}$. Indeed, by expanding the integrand of Eq. (4.6) at short distances, i.e. $\tilde{\ell}_r \ll 1$, we obtain

$$\Delta_r^{1/2} \frac{1}{2\ell_r^3} \left[-2 + \tilde{\ell}_r \left(\coth \tilde{\ell}_r + \tilde{\ell}_r \operatorname{csch}^2 \tilde{\ell}_r\right)\right] \simeq \Delta_r^{1/2} \frac{1}{\tilde{\beta}^3} \left[\frac{1}{45\tilde{\beta}} \ell_r - \frac{4}{945\tilde{\beta}^3} \ell_r^3 + \cdots\right]. \tag{4.7}$$

Only the 1-reflection path length can go to zero to generate a divergence. For this contribution Δ_r diverges like $1/\ell_r^2$ as $\ell_r \to 0$, however this is compensated by the ℓ_r term in (4.7) so the expression is finite and then integrable.

To check for infrared divergences notice that at large distances, $\tilde{\ell}_r \gg 1$, the integrand of (4.6) goes to $\Delta_r^{1/2}/\ell_r^2$. For an infinite flat plate the $\Delta_r \sim 1/z^2$, where z is the normal coordinate to the plate, and the integral is hence $\sim dz/z^3$ at large z. For finite plates the domain of integration is finite and for curved plates the enlargement factor falls even faster than $1/\ell^2$, and the integral remains convergent.

Since the integral converges in both the infrared and ultraviolet, it is safe to estimate the important regions of integration by naive dimensional analysis. This leads to the conclusion that '*The paths that dominate the temperature dependence of the Casimir force have lengths of order the thermal length* $\tilde{\beta}$'. High temperature implies short paths. Very low temperatures are sensitive to very long paths. Long paths involve both paths experiencing many reflections, which are sensitive to the actual dynamics at and inside the metallic surface, or paths making long excursions in an open geometry, which are sensitive to diffraction. Either way, low temperatures will present a challenge.

4.1.2. Parallel plates

We know that in the limit of infinite, parallel plates the optical approximation to the propagator becomes exact. Hence our method gives another way to calculate the free energy of this configuration of conductors. It is convenient to study this example to check against known results and to prepare the way for a study of the $T \to 0$ limit.

We recall that for this configuration the expression for the enlargement factor is $\Delta = 1/\square^2$ and the lengths are given by $\square_{2n} = 2na$ (where a is the distance between the plates) and $\square_{2n+1,u} = 2(a-z)+2na$, $\square_{2n+1,d} = 2z+2na$, the notation being the same as in Section 3.1, should at this point be familiar to the reader.

As in the zero temperature case it is useful consider even and odd reflection contributions separately and as for the zero temperature case, the sum over odd reflections turns into an integral over z from 0 to ∞

$$\begin{aligned}\mathcal{F}_{\text{odd}} &= \sum_{n=0}^{\infty} \mathcal{F}_{2n+1,d} + \mathcal{F}_{2n+1,u} \\ &= \frac{\hbar c}{2\pi^2 \tilde{\beta}^3} S \int_0^{\infty} dx \frac{1}{2x^4}\left[-2 + x\left(\coth x + x\,\mathrm{csch}^2 x\right)\right], \end{aligned} \tag{4.8}$$

where $x = 2z/\tilde{\beta}$ and S is the area of the plate. The definite integral can be easily performed numerically and its value is $\nu = 0.06089\ldots$,

$$\mathcal{F}_{\text{odd}} = 2\frac{\hbar c}{4\pi^2\tilde{\beta}^3} S\nu = \frac{\pi T^3}{2(\hbar c)^2} S\nu \tag{4.9}$$

which is independent of the separation, a, and therefore does not contribute to the force.

Let us turn now to the even reflection paths. They have constant length $2na$, so the volume integral simply yields the volume between the surfaces $V = Sa$. We already calculated the zero-reflection term $\mathcal{F}_0$ in Eq. (4.5). The remaining even reflection contributions (2, 4, 6, ... reflections) $\mathcal{F}_{\text{even},r\geqslant 2}$ can be written as an infinite sum

$$\mathcal{F}_{\text{even},r\geqslant 2} = -2\frac{\hbar c}{2\pi^2} Sa \frac{1}{\tilde{\beta}^4} \sum_{n=1}^{\infty} \frac{1}{2x_n^4}\left[-2 + x_n\left(\coth x_n + x_n\,\mathrm{csch}^2 x_n\right)\right] \tag{4.10}$$

where $x_n = 2na/\tilde{\beta} \quad n\tau$ (this defines the dimensionless temperature τ) and we have introduced an overall factor of two to take into account the multiplicity of the paths. Thus the total free energy for parallel plates is the sum of $\mathcal{F}_0$ (Eq. (4.5) and the results of Eqs. (4.9) and (4.10)),

$$\begin{aligned}\mathcal{F}_{\parallel} &= -\frac{\pi^4}{90}\frac{VT^4}{(\hbar c)^3} + \frac{\pi T^3}{2(\hbar c)^2} S\nu \\ &\quad - \frac{\hbar c}{\pi^2\tilde{\beta}^4} Sa \sum_{n=1}^{\infty} \frac{1}{2x_n^4}\left[-2 + x_n\left(\coth x_n + x_n\,\mathrm{csch}^2 x_n\right)\right]. \end{aligned} \tag{4.11}$$

It is not possible to rewrite $\mathcal{F}_{\parallel}$ in a closed form, but the sum is easy to compute numerically and the high and low temperature expansions are easy to obtain analytically. At high temperatures (and fixed a) $\tau \to \infty$, and the summand $g(n)$ in Eq. (4.11) falls rapidly enough with n

$$\begin{aligned} g(n) &= \frac{1}{2(\tau n)^4}\left[-2 + (\tau n)\left(\coth(\tau n) + (\tau n)\mathrm{csch}^2(\tau n)\right)\right] \\ &= \frac{1}{2(\tau n)^4}[-2 + \tau n] + \mathcal{O}\left(e^{-\tau n}\right), \end{aligned} \tag{4.12}$$

that the limit may be taken under the summation, with the result,

$$\mathcal{F}_{\text{even},r\geqslant 2} \simeq -\frac{hc}{\pi^2\tilde{\beta}^4}Sa\sum_{n=1}^{\infty}\left[\frac{1}{2n^3\tau^3}-\frac{1}{\tau^4 n^4}\right]=-\frac{\zeta(3)}{16\pi a^2}ST+\frac{\pi^2 hc}{1440a^3}S. \tag{4.13}$$

Notice that the second term cancels the even paths contribution to the Casimir energy. Hence the final expression for the high T expansion of the free energy is particularly simple,

$$\mathcal{F}_{\text{tot}}=\mathcal{F}+\mathcal{E}=-\frac{\pi^2}{90hc}VT^4+\nu\frac{\pi}{2(hc)^2}ST^3-\frac{\zeta(3)}{16\pi a^2}ST+\mathcal{O}\left(e^{-\pi Ta/hc}\right). \tag{4.14}$$

The first term is usual black body contribution to the bulk free energy. It does not contribute to the force. The second term is also independent of a and does not give rise to any force. The third term instead gives the thermal Casimir force. Notice that hc has disappeared from this expression. Called the "classical limit", this high temperature behavior has been noted before and some early results are even due to Einstein (in [26, p. 2]; see also [13]). In the next section, after the thermal corrections to the pressure are calculated, we show how to extend this result to other geometries.

Note some interesting features of the $T\to\infty$ limit: First, the sum over paths converges like the sum of $(1/n)^3$ as indicated by the appearance of $\zeta(3)$. While slower than the $T=0$ convergence, it is still rapid enough to obtain a good approximation from low reflections. Second, note that the $T\to\infty$ problem in 3-dimensions corresponds exactly to a $T=0$ problem in 2-dimensions. This is an example of the familiar dimensional reduction expected as $T\to\infty$. We can give a short proof of this result. Let us first write:

$$F=-\frac{1}{\beta}\log Z \tag{4.15}$$

where Z is the partition function. We need to evaluate Z to the lowest order in β when $\beta\to 0$. The thermal scalar field theory can be written as a free theory on the cylinder $\mathbb{R}^3\quad[0,\beta)$. For $\beta\to 0$ the dynamics along the thermal coordinate is frozen in the ground state, with energy $E_0=0$, where φ does not depend on the thermal coordinate. The partition function Z is now $Z=Z_3+\mathcal{O}(e^{-\beta E_1})$ where E_1 is the first excited state $E_1\propto 1/\beta^2$ and Z_3 is the partition function of the remaining three-dimensional problem in $\mathbb{R}^3$. If the conductors geometry is symmetric along one spatial coordinate, say x (in the parallel plates problem we have two of these directions, x and y) this can now be interpreted as an Euclideanized time variable extending from 0 to L_x/c. So we will write $Z_3=Z_{2+1}=e^{-\frac{1}{\hbar}\mathcal{E}_2 L_x/c}$ where $\mathcal{E}_2$ is the Casimir energy of the 2-dimensional problem of two lines of length L_y, distant a. The free energy F is then:

$$F=-\frac{1}{\beta}\log Z\simeq-\frac{1}{\beta}\log Z_{2+1}=T\frac{1}{\hbar}\frac{L_x}{c}\mathcal{E}_2=-TL_xL_y\frac{\zeta(3)}{16\pi^2a^2}. \tag{4.16}$$

Since $S=L_xL_y$ This is exactly the a-dependent term in Eq. (4.14). If the geometry is not translational invariant then we can only say from Eq. (4.16) that the free energy is linear in T (since Z_{2+1} is independent of β). Later, by using the optical approximation we will find an explicit analytic expression valid also for non-symmetric, smooth geometries.

For low temperatures, $\tau\to 0$, the terms in the n-sum in Eq. (4.11) differ very little from each other so we can use the Euler–Maclaurin formula [25],

$$\sum_{n=1}^{\infty} g(n) = \int_0^{\infty} dx\, g(x) - \frac{1}{2}g(0) - \frac{1}{12}g'(0) + \cdots = \frac{\nu}{\tau} - \frac{1}{90} + \mathcal{O}(\tau). \tag{4.17}$$

Substituting into Eq. (4.11) we find that the first term in Eq. (4.17) cancels the sum over odd reflections (the second term in Eq. (4.11)) and that the second term in Eq. (4.17) combines with $\mathcal{F}_0$ to give a very simple result,

$$\mathcal{F}_{\rm tot} = \mathcal{E} - \frac{(V - Sa)\pi^2 T^4}{90(hc)^3} \tag{4.18}$$

at low temperatures. This has a simple physical interpretation: the typical thermal excitations of the field at low temperature have very long wavelengths, it is hence energetically inconvenient for them to live between the two plates. As a result the only modification of the $T = 0$ result is to exclude from the standard black body free energy the contribution from the volume between the plates. One could imagine measuring this effect as a diminished heat capacity for a stack of conducting plates inside a cavity.

The low temperature result, Eq. (4.18), is deceptively simple. Its simplicity obscures an underlying problem with the $T \to 0$ limit. We postpone further discussion until we have explored the temperature dependence of the pressure. Suffice it to say for the moment, that Eq. (4.18) probably does not apply to realistic conductor with finite absorption, surface roughness, and other non-ideal characteristics.

4.2. Temperature dependence of the pressure

In this section we will obtain the temperature dependence of the pressure within our approximation and apply it to a preliminary study of the sphere and plate case. To begin, we calculate the thermal average of an operator $\mathcal{O}$ quadratic in the real scalar field φ. The average of a generic operator $\mathcal{O}$ is given by the trace over a complete set of eigenstates $|\Psi_\alpha\rangle$ of the Hamiltonian weighted by a Boltzmann factor:

$$\langle \mathcal{O} \rangle_T = \sum_\alpha e^{-\beta \mathcal{E}_\alpha} \langle \Psi_\alpha | \mathcal{O} | \Psi_\alpha \rangle. \tag{4.19}$$

After some algebra we find

$$\langle \mathcal{O} \rangle_T = \sum_j \mathcal{O}_j \langle 2n_j + 1 \rangle_T = \sum_j \mathcal{O}_j \frac{1 + e^{-\beta E_j}}{1 - e^{-\beta E_j}} \tag{4.20}$$

where $\langle\rangle_T$ denotes the thermal average, j labels the normal modes ψ_j (cf. Section 2), n_j is the occupation number of the mode j and E_j its energy. The quantities $\mathcal{O}_j$ are read from the decomposition of the diagonal part of the operator $\mathcal{O}$ written as $\mathcal{O}_{\rm diag} = \sum_j \mathcal{O}_j (a_j^\dagger a_j + a_j a_j^\dagger)$ where a_j is the annihilation operator of the mode j.

The $\mathcal{O}_j$ for the pressure can be read easily from the analysis in Section 2:

$$P_j = \lim_{x' \to x \in \mathcal{S}} \frac{1}{4E_j} \partial'_{\hat{n}} \partial_{\hat{n}} \psi_j(x') \psi_j(x). \tag{4.21}$$

So we can write the pressure on the plate at non-zero temperature as

$$
\begin{aligned}
P(x \in \mathcal{S}) &= \lim_{x' \to x} \sum_j \frac{1}{4E_j} \partial'_n \partial_n \psi_j(x') \psi_j(x) \left(\frac{1 + e^{-\beta E_j}}{1 - e^{-\beta E_j}} \right) \\
&= \lim_{x' \to x} \partial'_{\tilde{n}} \partial_{\tilde{n}} \int_0^\infty dk\, e^{-k/\Lambda} \frac{k}{2\pi E(k)} \operatorname{Im} G(x', x, k) \left(\frac{1 + e^{-\beta E(k)}}{1 - e^{-\beta E(k)}} \right) \\
&= \operatorname{Im} \int_0^\infty dk\, e^{-k/\Lambda} \frac{k}{2\pi E(k)} \frac{1}{2} \partial^2_{\tilde{n}}\, G(x, x, k) \left(\frac{1 + e^{-\beta E(k)}}{1 - e^{-\beta E(k)}} \right)
\end{aligned}
\tag{4.22}
$$

where we have used Eq. (2.30).

Next we introduce the optical approximation for the propagator and limit ourselves to massless scalars $E(k) = \hbar c k$. The discussion of the divergences parallels that of Section 2 and needs not be repeated here. We remove P_0 and P_1 and leave all the finite contributions $r \in \mathcal{R}$. The optical approximation for the pressure exerted by a massless scalar field reads

$$
P(x) = \sum_{r \in \mathcal{R}} (-1)^{n_r} \partial^2_{\tilde{n}} \frac{\Delta_r^{1/2}}{16\pi^2} \left[\frac{1}{\tilde{\beta}} \coth(\ell_r / \tilde{\beta}) \right],
\tag{4.23}
$$

where it is understood that the zeroth and first reflection terms, which contribute to the pressure on each surface individually, but not to the force between surfaces, have been dropped.

Before applying this to the sphere and plate problem, let us again look at the limiting behavior as $T \to \infty$ and $T \to 0$, and draw some conclusions independent of the detailed geometry. First consider $T \to \infty$. The shortest paths in the sum in Eq. (4.23) are of order a, the intersurface separation. (Remember that the optical approximation is accurate as long as the important paths are short compared to R, a typical radius of curvature of the surfaces.) At high T we can take the $\tilde{\beta} \to 0$ limit under the sum over reflections since the resulting sum still converges. Therefore low reflections dominate, and we can see, retrospectively, that the high temperature approximation applies when $\tilde{\beta}/a \to 0$. So as $T \to \infty$,

$$
P = \sum_r (-1)^{n_r} \partial^2_{\tilde{n}} \frac{\Delta_r^{1/2}}{16\pi^2} \left[\frac{1}{\tilde{\beta}} + \mathcal{O}\left(\frac{1}{\tilde{\beta}} e^{-\ell_r / \tilde{\beta}} \right) \right].
\tag{4.24}
$$

This limit has been called (it has been previously found for the parallel plates case) the "classical limit" [3,13,26], since the final expression for high temperatures, reinserting $\hbar$ and c,

$$
P \simeq \sum_r (-1)^{n_r} \partial^2_{\tilde{n}} \frac{\Delta_r^{1/2}}{16\pi} T
\tag{4.25}
$$

is independent of $\hbar$ and c apart from exponentially small terms. This expression amounts in neglecting the 1 in the expression $\langle 2n_j + 1 \rangle_T$, corresponding to normal ordering or neglecting the contribution of the vacuum state.

At low temperatures, $\tilde{\beta} \to \infty$, it is not possible to interchange the limit with the sum. The relevant quantity is $\frac{1}{\tilde{\beta}} \coth(\ell_r / \tilde{\beta})$, which goes like

$$
\frac{1}{\tilde{\beta}} \coth\left(\frac{\ell_r}{\tilde{\beta}} \right) = \frac{1}{\ell_r} + \frac{\ell_r}{3\tilde{\beta}^2} - \frac{\ell_r^3}{45\tilde{\beta}^4} + \mathcal{O}\left(\frac{\ell_r^5}{\tilde{\beta}^4} \right)
\tag{4.26}
$$

as $\tilde{\beta} \to \infty$. The first term yields the familiar $T = 0$ expression. The others would give divergent contributions because of the factors of ζ_r in the numerators (even after the inclusion of the enlargement factor Δ_r). Of course the sum over reflections of the *difference*, $\frac{1}{\tilde{\beta}} \coth(\zeta_r/\tilde{\beta}) - \frac{1}{\zeta_r}$, converges to zero as $\tilde{\beta} \to \infty$, so thermal corrections definitely vanish for any geometry as $T \to 0$ as expected. Once again we relegate more detailed consideration of the $T \to 0$ limit to a later subsection.

4.2.1. Sphere and plate

In this section we calculate the pressure and total force for the configuration of a sphere facing a plane at non-zero temperature within 5p reflections. The optical approximation should be accurate if the important paths are short compared to R, the radius of the sphere. On the other hand the thermal corrections to the force are sensitive to paths with lengths of order $\tilde{\beta}$. So we must have $R \gg \tilde{\beta}$ and $R \gg a$ in order to obtain reliable results from the optical approximation. Fortunately this is a region of experimental interest: present experiments use, for example, $a \sim 0.5$ μm, $R \sim 100$ μm, and at room temperature, $\tilde{\beta} \sim 2.5$ μm. In this regime the optical approximation should give a good description of the thermal corrections to the force between perfectly reflective, perfectly smooth conductors.

The expression for the pressure is given by Eq. (4.23), the enlargement factors and lengths are the same as in the $T = 0$ case. By applying Eq. (4.23) to the 1s + 3s paths we find the results in Fig. 6. Notice that at high temperatures increasing the temperature essentially scales the whole plot proportionally to T. The force is then linearly dependent on the temperature (this is the 'classical limit' already discussed in Section 4.2). More details are given in the caption of Fig. 6.

A dimensionless function $f(a/R, \tilde{\beta}/R)$ can again be defined by rescaling the total force F to extract the leading term as $a \to 0$. The limiting behavior $a \to 0$ is not affected by temperature effects so we stick to the old definition for f:

$$F(a, \tilde{\beta}, R) = -\frac{hc\pi^3 R}{720 a^3} f(a/R, \tilde{\beta}/R). \tag{4.27}$$

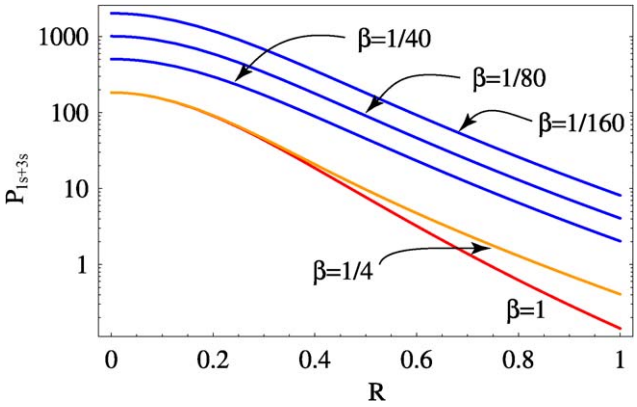

Fig. 6. (Colour online.) The ρ dependence of the 1s + 3s contribution to the pressure P_{1s+3s} for the sphere and the plate in units of hc/R^4 for various temperatures. Two effects must be noticed. The top 3 curves (in blue) show the high-temperature region where the pressure is proportional to T (notice the logarithmic scale). The two lower curves (in orange and red) show the low-temperature region when increasing the temperature changes the asymptotic behavior of P for large ρ (i.e. $\rho \gtrsim \tilde{\beta}$) while for small ρ the behavior reduces to the zero-temperature limit.

In Fig. 7 we present f (up to 5 reflections) for 5 different values of $\tilde{\beta}/R$ (we choose 1, 1/2, 1/4, 1/8 and 1/16 recognizing that $\tilde{\beta} \quad 1$ strains the limits of our approximations) and varying a. Notice that in a neighborhood of $a/R = 0$, shrinking as $\tilde{\beta}/R$ increases, the function f is very well approximated by the $T = 0$ form, already discussed in Section 3.3, $f(a/R) \simeq 1 - 0.1a/R$. It is not useful to study the derivative $A(\tilde{\beta}/R) = \partial f(x, \tilde{\beta})/\partial x$ as $x = a/R \to 0$ since this will take the constant value predicted by the zero temperature analysis, or -0.1 in this approximation, for any value of the temperature we choose.

It is also clear from the previous discussions leading to Eq. (4.24) that in the opposite regime, for $a/\tilde{\beta} \blacktriangleleft 1$, we must have $F \propto R/a^2\tilde{\beta} = RT/a^2$ (the 'classical limit'). In fact, the first term in the high temperature expansion (4.24) integrated over ρ converges and gives a finite force linear in T. For this problem, the first term in the reflection expansion for high temperatures can even be calculated analytically:

$$F_{1s+3s} = -\hbar c \frac{R}{8\pi a^2 \tilde{\beta}} + \mathcal{O}\left(e^{-R/\tilde{\beta}}\right) \simeq -\hbar c \frac{R}{8a^2} T. \tag{4.28}$$

Unfortunately there is no such simple closed expression for higher reflection terms (nor for this first term at arbitrary T). However, if one believes that the rank of contributions is similar to the parallel plates case one should feel safe to say that this truncation captures the optical approximation within a $\zeta(3) - 1 \simeq 20\%$. Hence our statements are at least *qualitatively* correct.

This expression for the force gives a prediction for the function f, defined in Eq. (4.27). At this level of accuracy ($1s + 3s$ reflection) and for $a/\tilde{\beta} \gtrsim 1$, apart for exponentially small terms in the temperature expansion we have

$$f_{1s+3s} \simeq \frac{90}{\pi^4} \frac{a}{R} \frac{R}{\tilde{\beta}} \tag{4.29}$$

which grows linearly in a/R and is (interestingly enough) independent of R. This is evident in Fig. 7 for the curves with $\tilde{\beta} = 1/8,\ 1/16$. For higher $\tilde{\beta}$ the linear growth starts at higher values of a not shown in Fig. 7. Moreover the exponential accuracy manifests itself in the sudden change of behavior from $f \simeq 1 - 0.1a/R$ to $f \propto a/\tilde{\beta}$.

It is quite easy to extract a universal prediction from this data, whatever the definitive numbers are, after the sum over optical paths is carried to sufficiently high order: *for any non-zero tem-*

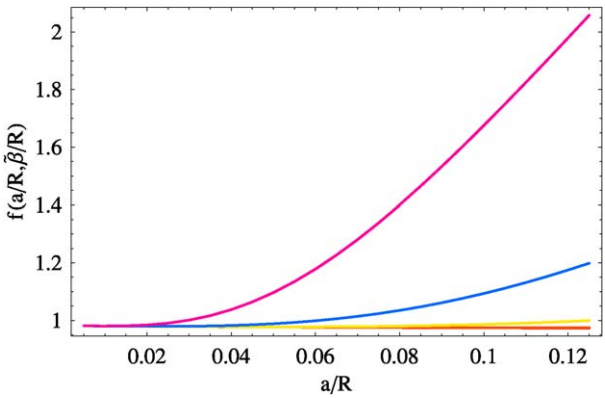

Fig. 7. (Colour online.) The function $f(a/R, \tilde{\beta}/R)$ as a function of a/R for $\tilde{\beta}/R$ (from red to violet or down up) $= 1, 1/2, 1/4, 1/8, 1/16$. $f(0) \simeq 0.98$ since we are summing only up to reflection $5p$. The two lowermost curves, red and orange ($\tilde{\beta} = 1, 1/2$) superpose almost exactly.

perature the function $f(a/R)$ *will deviate from his zero-temperature behavior at* $a \gtrsim \tilde{\beta}$ hc/T. *The deviation will be in the upward direction, increasing the attractive force between the bodies*. Eventually, for sufficiently large distances, the high temperature behavior given by Eq. (4.25) (or (4.29) for the sphere-plane problem) will be recovered.

4.3. Thermal corrections at low temperatures

The preceding examples have made it clear that in the language of the optical approximation, thermal corrections at low temperature arise from very long paths, ℓ_r $\tilde{\beta}$. This can be seen from the general form of the free energy, Eq. (4.6), or in the attempt to take the $\tilde{\beta} \to \infty$ limit under the summation in Eq. (4.23), which fails because of the expansion, Eq. (4.26). Here we examine this non-uniformity more carefully in general and in particular for the parallel plate case, where all the expressions are available. We then attempt to draw some conclusions about the magnitude of corrections at low temperature and the possibility of calculating them reliably in an model that idealizes the behavior of materials.

We return to Eq. (4.22), which gives the exact expression for the pressure, and separate out the thermal contribution,

$$P(T) - P(0) \quad \delta P = \mathrm{Im} \int_0^\infty dk \frac{1}{2\pi} \partial^2_{n'n} \mathcal{G}(x', x, k) 2 \frac{e^{-\beta hck}}{1 - e^{-\beta hck}}, \tag{4.30}$$

still exact. Expanding the denominator in a geometric series, we find

$$\delta P = \frac{1}{\pi} \mathrm{Im} \sum_{m=1}^{\infty} \int_0^\infty dk\, \partial^2_{n'n} \mathcal{G}(x', x, k) e^{-m\beta hck}. \tag{4.31}$$

Each term in the sum is a Laplace transform of the Greens function. Clearly, as $\beta \to \infty$ the frequencies that dominate this integral are $\propto 1/\beta$ T.

What are the low frequency contributions to $\mathcal{G}(x', x, k)$? In the ideal case of infinite, perfectly conducting, parallel plates, there is a gap in the spectrum at low k: $k \geqslant \frac{\pi}{a}$. However *in realistic situations* the plates are finite and/or curved, the geometry is open, and there is no gap in the spectrum. The low-k part of the spectrum is sensitive to the global geometry, including edges and curvature, and to the low frequency properties of the material. If the conditions are close to the ideal, the contributions to δP from small k may be small. However as $T \to 0$, they dominate. We conclude that the $T \to 0$ behavior of δP cannot be calculated for realistic situations.

The optical approximation does not take account of diffraction, and cannot accurately describe the $T \to 0$ limit. Nevertheless it is interesting to see how it fails, since this sheds light on the problem in general. Substituting the optical expansion for the Greens function (replacing $\partial^2_{n'n} \to \frac{1}{2}\partial_z^2$ and setting $h = c = 1$) we find

$$\begin{aligned} \delta P &= -\sum_{m=1}^{\infty} \sum_{r \geqslant 1} \frac{1}{8\pi^2} \partial_z^2 \int_0^\infty dk\, \Delta_r^{1/2} \sin(k\ell_r) e^{-m\beta k} \\ &= -\sum_{m=1}^{\infty} \sum_{r \geqslant 1} \frac{1}{8\pi^2} \partial_z^2 \Delta_r^{1/2} \frac{\ell_r}{m^2\beta^2 + \ell_r^2}. \end{aligned} \tag{4.32}$$

plates approximation, extended to curved geometries by means of the PFA, and a derivation (like ours) in which the curvature is inserted ab initio. The thermal and curvature scales interplay in a way that the usual derivations [3,4] could not possibly capture, giving rise to different power law corrections in a/β. It is worth reminding the reader that the usual numerical estimates of thermal corrections are based on the infinite parallel plates power law $(a/\beta)^4$. A smaller power like $(a/\beta)^2$ would give a much bigger upper bound.

To summarize: temperature corrections are small at small T, but the existing methods of calculating them, including both our optical approximation and the traditional parallel plates idealization, cannot be trusted to give a reliable estimate of the T-dependence at small T.

5. Conclusions

In this paper we have shown how to adapt the optical approximation to the study of local observables. We have illustrated the method by studying the pressure, but the method applies as well to other components of the stress tensor, to charge densities, or any quantity that can be written in terms of the single particle Greens function. The advantage of the optical approximation is to extend the study of these local observables to novel geometries. In particular we developed an expression for the Casimir pressure on the bodies and applied our main result Eq. (2.31) to the study of three important examples: parallel plates, the Casimir pendulum and a sphere opposite a plate.

We have also shown how to calculate within this approximation scheme, thermodynamic quantities and thermal corrections to the pressure in the general case and applied our results to the example of parallel plates (retrieving the known results) and to the case of a sphere opposite a plate. Along the way we have given a proof of the "classical limit" of Casimir force for any geometry (within our approximation), i.e. the fact that Casimir forces at high temperatures are proportional to the temperature and independent of $\hbar$, a fact that previously was known only for parallel plates.

Finally, we argued that all known methods of computing the temperature dependence of the Casimir effect are suspect as $T \to 0$.

Acknowledgements

We would like to thank S. Fulling and M. Schaden for comments. A.S. would like to thank M.V. Berry for useful discussions. R.L.J. would like to thank the Rockefeller Foundation for a residency at the Bellagio Study and Conference Center on Lake Como, Italy, where much of this work was performed. This work is also supported in part by funds provided by the US Department of Energy (D.O.E.) under cooperative research agreement DE-FC02-94ER40818.

References

[1] H.B.G. Casimir, Proc. K. Ned. Akad. Wet. 51 (1948) 793.
[2] E.M. Lifshitz, Sov. Phys. JEPT 2 (1956) 73;
N.E. Dzyaloshinskii, E.M. Lifshitz, L.P. Pitaevskii, Sov. Phys. Usp. 4 (1961) 152;
L.D. Landau, E.M. Lifshitz, Electrodynamics of Continuous Media, Pergamon, Oxford, 1960.
[3] V.M. Mostepanenko, N.N. Trunov, Casimir Effects and Its Applications, Oxford Univ. Press, 1997.
[4] R.S. Decca, E. Fischbach, G.L. Klimchitskaya, D.E. Krause, D.L. Lopez, V.M. Mostepanenko, Phys. Rev. D 68 (2003) 116003, hep-ph/0310157.
[5] S.K. Lamoreaux, Phys. Rev. Lett. 78 (1997) 5;

M. Bordag, U. Mohideen, V.M. Mostepanenko, Phys. Rep. 353 (2001) 1, quant-ph/0106045;
G. Bressi, G. Carugno, R. Onofrio, G. Ruoso, Phys. Rev. Lett. 88 (2002) 041804.
[6] N. Graham, R.L. Jaffe, V. Khemani, M. Quandt, M. Scandurra, H. Weigel, Nucl. Phys. B 645 (2002) 49, hep-th/0207120.
[7] R. Golestanian, M. Kardar, Phys. Rev. A 58 (1998) 1713, quant-ph/9802017;
T. Emig, cond-mat/0311465;
T. Emig, Europhys. Lett. 62 (2003) 466, cond-mat/0206585;
R. Buscher, T. Emig, cond-mat/0401451.
[8] H. Gies, K. Langfeld, L. Moyaerts, JHEP 0306 (2003) 018, hep-th/0303264.
[9] A recent review for the mathematically minded reader is: A. Uribe, Trace formulae, in: S. Perez-Esteva, C. Villegas-Blas (Eds.), First Summer School in Analysis and Mathematical Physics: Quantization, the Segal–Bargmann Transform and Semiclassical Analysis, in: Contemporary Mathematics, vol. 260, American Mathematical Society, Providence, 2000, pp. 61–90.
[10] R.L. Jaffe, A. Scardicchio, Phys. Rev. Lett. 92 (2004) 070402, quant-ph/0310194.
[11] A. Scardicchio, R.L. Jaffe, Nucl. Phys. B 704 (2005) 552, quant-ph/0406041.
[12] M.V. Berry, J. Phys. A 5 (1972) 272–291.
[13] J. Feinberg, A. Mann, M. Revzen, Ann. Phys. 288 (2001) 103, hep-th/9908149.
[14] N.D. Birrell, P.C.W. Davies, Quantum Fields In Curved Space, Cambridge Univ. Press, Cambridge, 1982.
[15] See for example, S. Weinberg, The Quantum Theory of Fields, Cambridge Univ. Press, Cambridge, 1996.
[16] B.V. Derjagin, Kolloid Z. 69 (1934) 155;
B.V. Deriagin, I.I. Abrikosova, E.M. Lifshitz, Sov. Phys. JETP 3 (1957) 819;
For a modern discussion of the Proximity Force Approximation, see: J. Blocki, W.J. Swiatecki, Ann. Phys. 132 (1981) 53.
[17] G. Barton, J. Phys. A 37 (2004) 1011–1049;
R.L. Jaffe, AIP Conf. Proc. 687 (2003) 3, hep-th/0307014.
[18] S. Reynaud, A. Lambrecht, C. Genet, in: K. Milton (Ed.), Quantum Field Theory under the Influence of External Boundaries, Rinton Press, 2004, p. 36.
[19] M. Born, E. Wolf, Principles of Optics, Cambridge Univ. Press, Cambridge, 1980.
[20] R.L. Jaffe, A. Scardicchio, JHEP 0506 (2005) 006, hep-th/0501171.
[21] M. Schaden, L. Spruch, Phys. Rev. A 58 (1998) 935;
M. Schaden, L. Spruch, Phys. Rev. Lett. 84 (2000) 459.
[22] J.B. Keller, J. Opt. Soc. Am. 52 (1962) 116;
J.B. Keller, in: Calculus of Variations and its Application, American Mathematical Society, Providence, 1958, p. 27;
B.R. Levy, J.B. Keller, Commun. Pure Appl. Math. XII (1959) 159;
B.R. Levy, J.B. Keller, Can. J. Phys. 38 (1960) 128.
[23] M. Schaden, L. Spruch, cond-mat/0304290.
[24] H.B.G. Casimir, D. Polder, Phys. Rev. 73 (1948) 360.
[25] M. Abramowitz, I. Stegun, Handbook of Mathematical Functions, Dover, New York, 1970.
[26] P.W. Milonni, The Quantum Vacuum: An Introduction to Quantum Electrodynamics, Academic Press, London, 1994.